

# Emptying Bottles: A Study of Glugging

Zachary A. Kenton\*

Jerome A. Neufeld

Herbert E. Huppert

September 6, 2012

---

\*Funded by Bridgwater Fund. Contact: zakenton@gmail.com

# Experiment 1: Emptying Bottles

## Setup: Experiment 1

A schematic of the experimental setup used to measure the emptying time,  $T_e$ , of each bottle is shown in Figure 1. Water is initially contained in the bottle which is inclined at an angle (in degrees)  $0 \leq \theta \leq 90$  to the horizontal. Below is a jug sitting on a mass balance. The jug contains sponges to absorb the water, minimising splashing and the inertia of the water.

The geometrical properties of the bottles used are summarised in Table 1, and the properties of the bungs used are shown in Table 2. The physical characteristics of the fluid ( $\rho, \nu, \sigma, g$ ) remained the same.

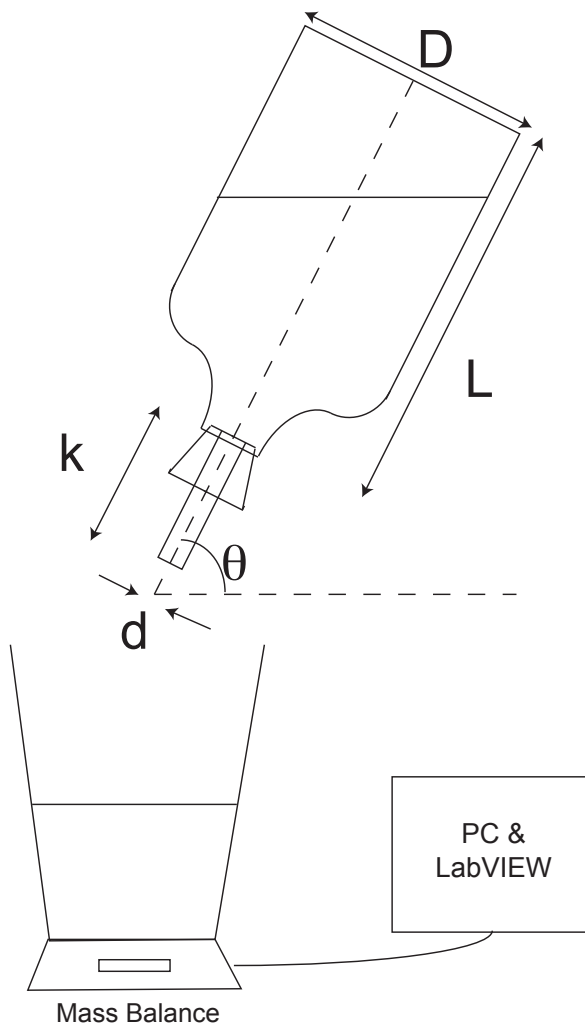


Figure 1: Schematic

Table 1: Geometrical Properties of Bottle

| Bottle       | Total Volume $V$ (L) | Length $L$ (m) | External Diameter Body $D$ (m) | Internal Diameter Neck $d$ (open) (m) |
|--------------|----------------------|----------------|--------------------------------|---------------------------------------|
| 1 (Wine)     | 0.77                 | 0.284          | 0.075                          | 0.020                                 |
| 2 (Jeroboam) | 3.03                 | 0.472          | 0.134                          | 0.018                                 |

Table 2: Geometrical Properties of Bung

| Bung | Tube Length $k$ (m) | Internal Diameter $d$ (m) |
|------|---------------------|---------------------------|
| 1    | 0.028               | 0.013                     |
| 2    | 0.028               | 0.010                     |
| 3    | 0.028               | 0.009                     |

## Results: Experiment 1

### Bottle 1: Standard Wine Bottle

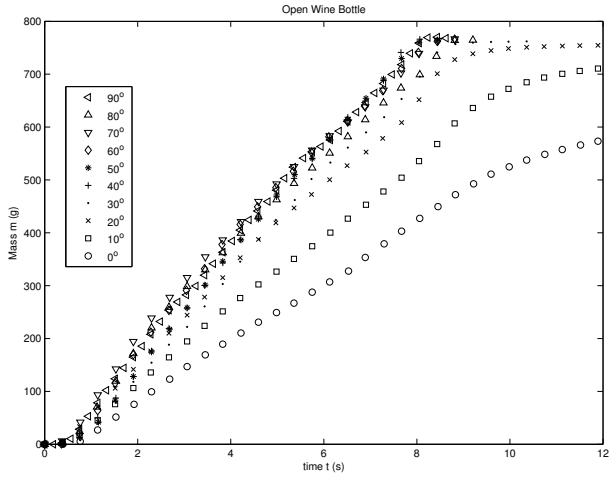
In Figure 2 we plot the mass in the jug against time, for various angles, and at various exit diameters.

In Figure 2a, with an open necked bottle, we see an almost constant flux for each angle, with slight acceleration just towards the end of emptying in the low angles  $0 \leq \theta \leq 30$ , this occurs when the upper free surface reaches the level of the neck, and a continuous stream of water exits the bottle, without glug-glug. The total emptying time,  $T_e$  reaches a minimum at around  $\theta = 40$ , after which increasing the angle slows the flow, due to the large air glugs entering the bottle. The slowest flow rates nonetheless, are at low angles (and these low angles don't even discharge the total volume of water contained in the bottle, due to pooling in the shoulder).

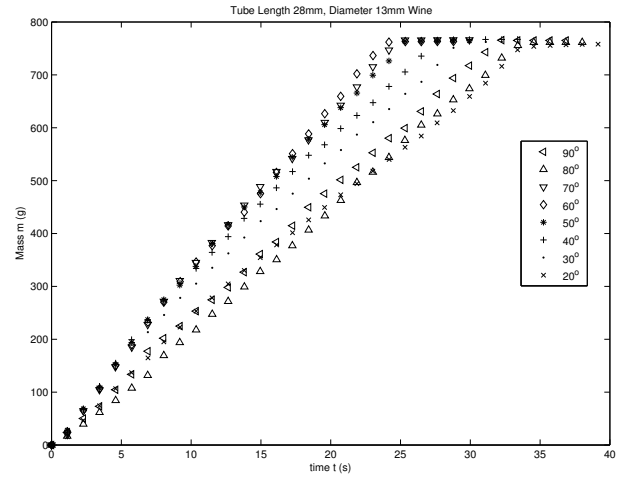
Figure 2b shows the results for a bung with a steel tube of length 28mm, diameter 13mm. There was no continuous flow for  $0 \leq \theta < 20$ .  $T_e$  reaches a minimum at around  $\theta = 60$ . We no longer see the acceleration towards the end of emptying at low angles as the free surface doesn't reach the level of the exit tube.

Figure 2c uses a thinner 10mm diameter exit tube. In this setup however, there was no continuous flow for  $90^\circ$ . We see the initial flow rate for each angle is equal, yet after about 20 seconds, the higher angles  $70 \leq \theta \leq 80$  seem to decelerate, while the others seem to decelerate less.  $\theta = 20$  doesn't seem to decelerate much at all, and ends up being the optimal angle for lowest  $T_e$ .

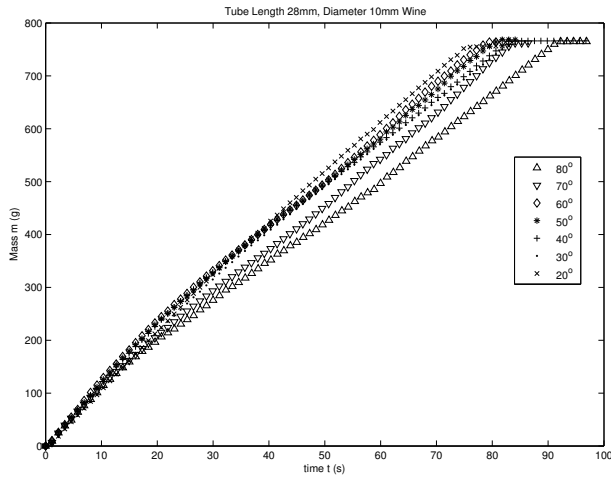
Figure 2d uses the thinnest 9mm tube diameter exit tube. No continuous flow for  $80^\circ$  or  $90^\circ$  was observed. The lowest  $T_e$  occurs for  $\theta = 40$ .



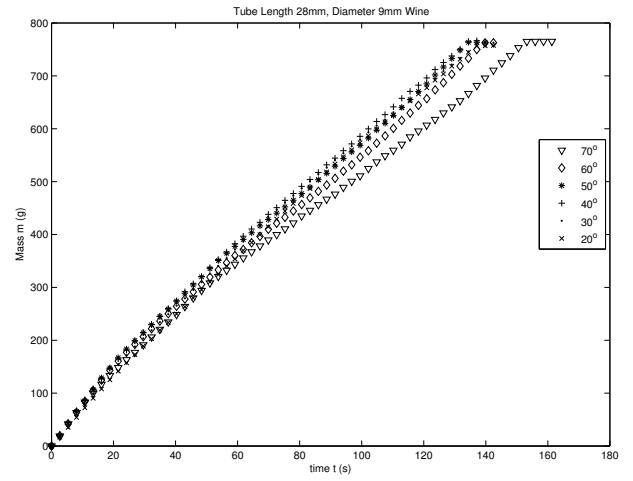
(a) Bottle 1, Open



(b) Bottle 1, Bung 1



(c) Bottle 1, Bung 2



(d) Bottle 1, Bung 3

Figure 2: Mass Flux

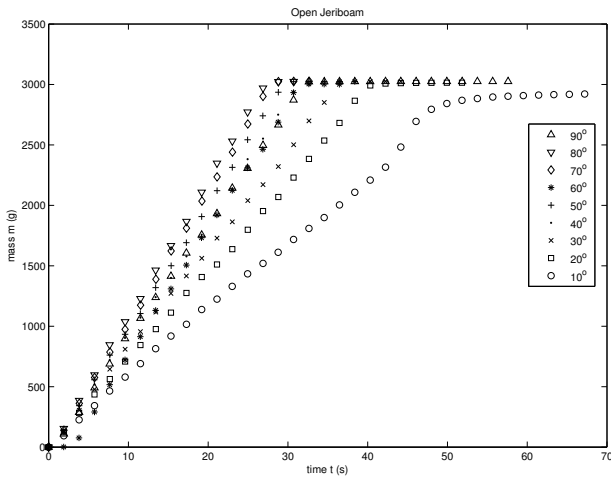
## Bottle 2: Jeriboam (Double Magnum)

In Figure 3 we again plot the mass in the jug against time, for various angles, and at various exit diameters for Bottle 2.

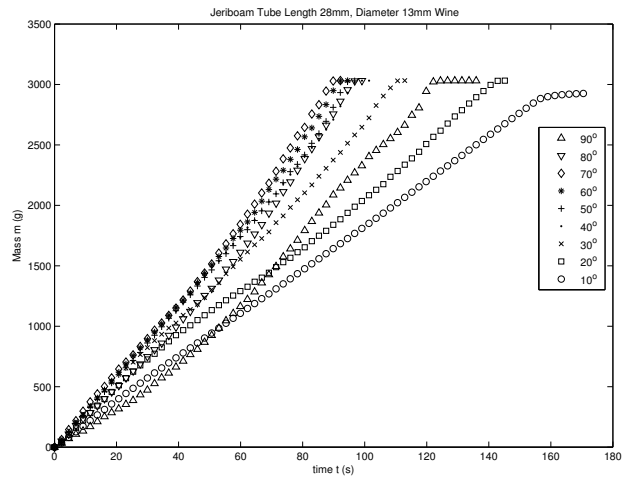
Figure 3a shows for the open bottle, increasing angle decreases  $T_e$  peaking at  $80^\circ$ , with  $90^\circ$  taking longer. All lines have constant gradient, except for  $10^\circ$  where we again see acceleration just towards the end of emptying, when the upper free surface reaches the level of the neck. Figure 3b shows similar behaviour over a longer timescale, peaking at around  $70^\circ$ .

Figure 3c shows some qualitatively different behaviour though. All angles begin with similar gradients but then each experiences an accelerated phase, after discharging around  $600g$ , in which the gradients increase, by amounts depending on the angle.  $20^\circ$  doesn't seem to be effected in this way, and continues without an abrupt acceleration phase. For the larger angles, there appears to be a third phase beginning at about  $2200g$ , in which the gradient increases again. Figure 3d exaggerates the behaviour over a longer timescale.

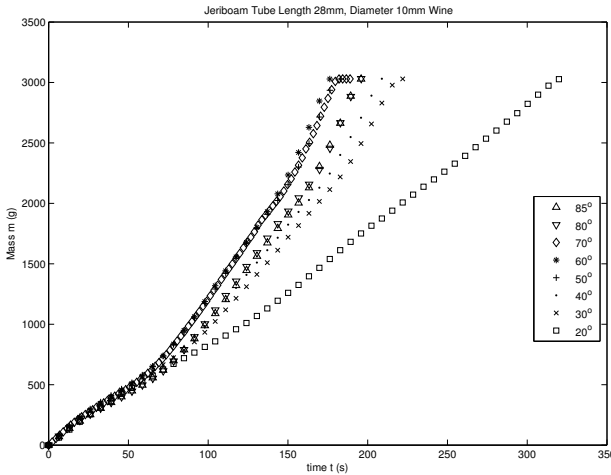
It appears for these constricted flows, we observe a new glugging regime after the water falls below a critical volume (discharging around  $600g$ ), at which the vacuum strength above the free surface is powerful enough to suck in more air, and hence allow more water out on the next glug, giving rise to the increase in gradient. The third phase is probably due to the gradual thinning of the neck, a geometrical effect rather than a dynamical one.



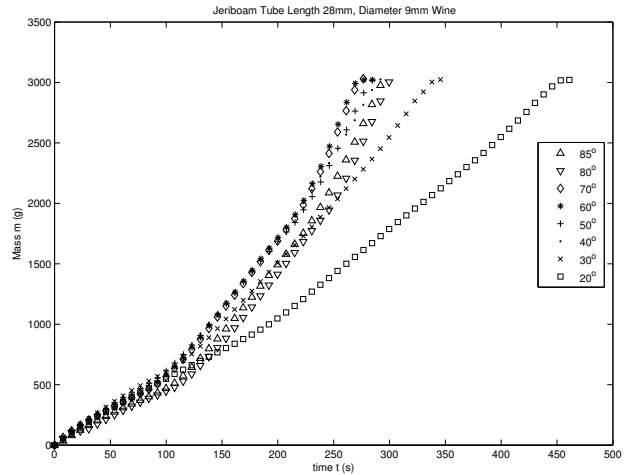
(a) Bottle 2, Open



(b) Bottle 2, Bung 1



(c) Bottle 2, Bung 2



(d) Bottle 2, Bung 3

Figure 3: Mass Flux

Figure 4 and Figure 5 show loglog plots of  $T_e$  versus  $d$ , for various angles. We note the strong power law, and find that for the individual bottle, the slopes of the lines are almost the same for each angle, with slopes for Bottle 1 being slightly larger than for those in Bottle 2. This is to be compared with Clanet and Searby (2004), where they obtained the experimental value of the slope to be -2.59, for the vertical case.

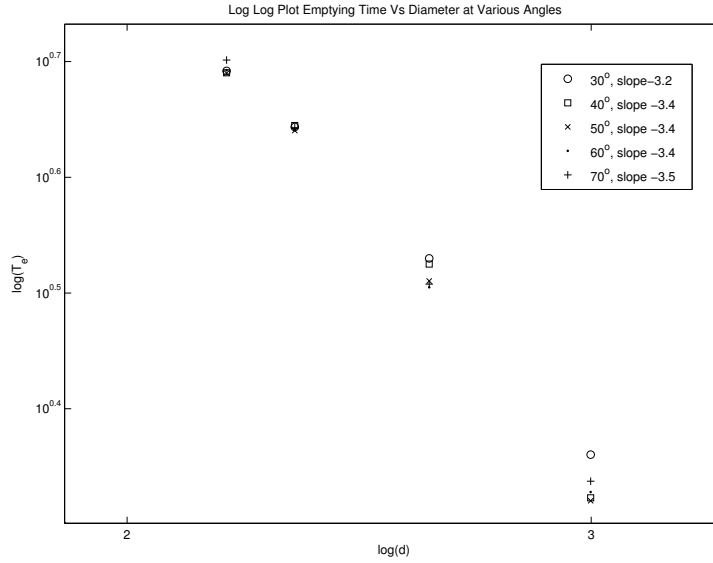


Figure 4: Bottle 1:  $T_e$  power law dependence on  $d$

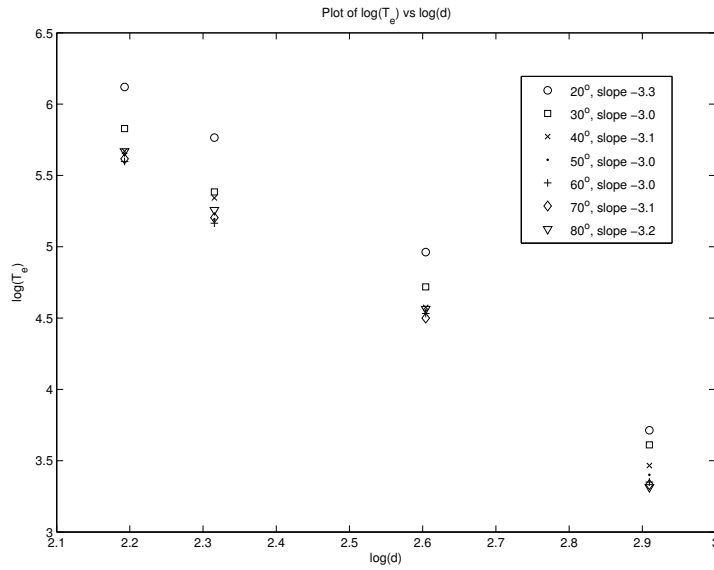


Figure 5: Bottle 2:  $T_e$  power law dependence on  $d$

## Experiment 2: Emptying a Tank

### Setup: Experiment 2

To exaggerate the effects of different glugging regimes, we design a slightly different experiment. Figure 6 shows a schematic for Experiment 2, using an upper cylindrical tank, of height  $H = 0.172m$ , diameter  $D = 0.16m$ , closed at the top, with a hole in the bottom, to which tubes of different diameters and lengths can be attached. Geometrical properties of the tubes used appear in Table 3.

The experiment begins with the tube and tank both full of water, and a bung is released from the bottom of the tube. As before, water is collected in a jug below the tube, placed on a mass balance connected to LabVIEW. We also attach a pressure sensor sealed into the top of the tank to measure differences in the air pressure above the water.

Table 3: Geometrical Properties of Tube

| Tube | Tube Length $L_1$ (m) | Internal Diameter Tube $d$ (m) |
|------|-----------------------|--------------------------------|
| 1    | 2                     | 0.010                          |
| 2    | 1                     | 0.010                          |
| 3    | 0.5                   | 0.010                          |
| 4    | 0.2                   | 0.010                          |
| 5    | 0.1                   | 0.010                          |
| 6    | 0.02                  | 0.010                          |

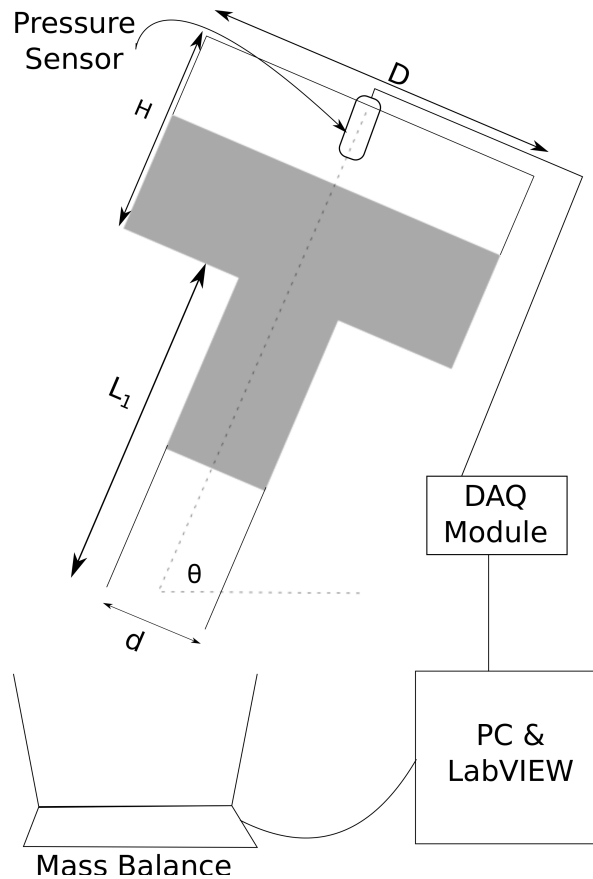


Figure 6: Schematic, Experiment 2

## Results: Experiment 2

We present a selection of the results obtained from experiment 2. We begin with our largest length tube, Tube 1, held vertically at  $\theta = 90^\circ$ . Figure 7 shows the time evolution of the mass collected, and the corresponding pressure in the tank. The initial large pressure drop at very early times is due to the bung being removed, allowing a large volume of water to escape, as can be seen by the large mass gradient. Air is then sucked back up the tube, allowing the pressure to rise.

The pressure then oscillates with small amplitude, and high frequency, while the mass steadily increases at constant low gradient, as exchange flow occurs at the hole where tube meets tank, and small bubbles of air are formed here. This first phase continues up to about 45s, which (after Huppert & Hallworth) we call ‘popping’ due to the acoustic signal emitted. In this phase, the air acts incompressibly, with the volume of water discharged being replaced by the same volume of air.

Between 45s and 130s exchange flow occurs in the tube, rather than at the hole, in a second phase called ‘glugging’. This gives a larger amplitude pressure oscillation, at a slightly lower frequency, with a slightly increased mass gradient. The maximum length of drawdown steadily increases until it attains the full length of the tube, at about 130s. This is due to the growing volume of air in the tank, which starts to behave in a more compressible way as it grows over many cycles.

After about 130s, the maximum length of drawdown achieves the full length of the tube, and allows exchange to occur at the end of the tube, rather than in tube. This phase is known as ‘slugging’. Exchange at the end of the tube allows a much larger discharge of water (as can be seen by the step-like nature of the mass plot), and violent drawback of water and excess air, which jets into the tank and over-pressurises the air above the water, which forces the water back down the tube with large force in the next slug. Simultaneously, the pressure oscillations grow to a very large amplitude, with a lower frequency, which matches the frequency of the steps of the mass plot. Minimum pressure is achieved in the middle of outflow of water, and a pressure maximum spike occurs when the water and air jet back into the tank, when no outflow occurs. This cycle repeats, until all the water has drained from the tank.

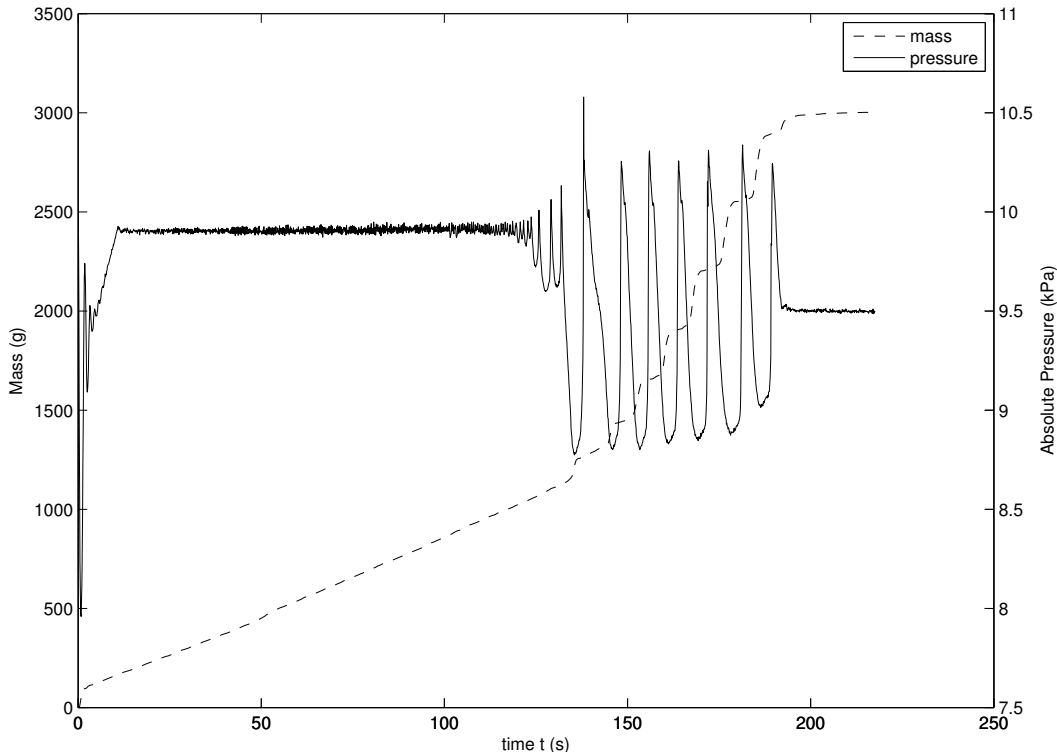
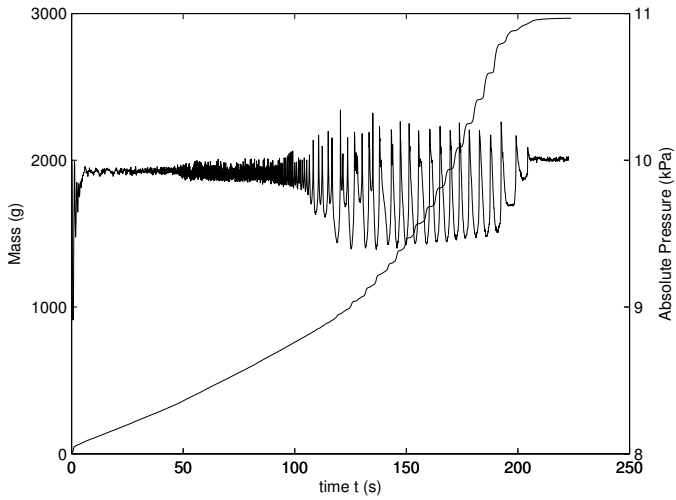
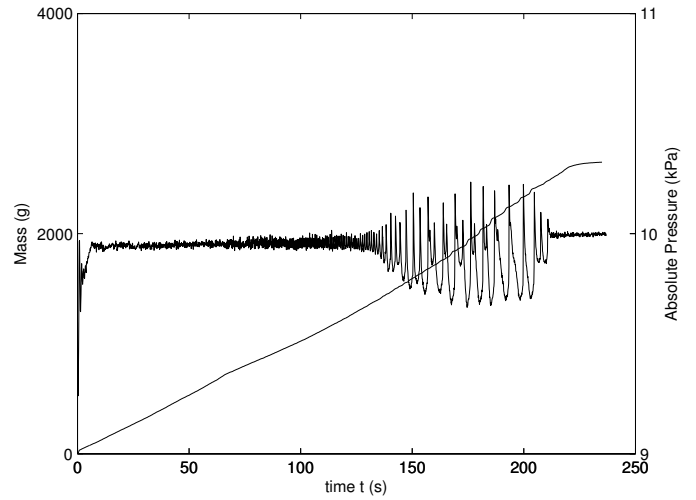


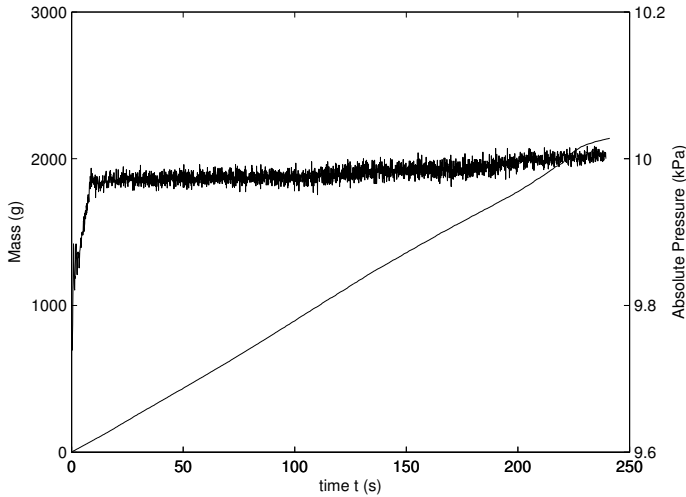
Figure 7: Tank, Tube 1,  $\theta = 90^\circ$



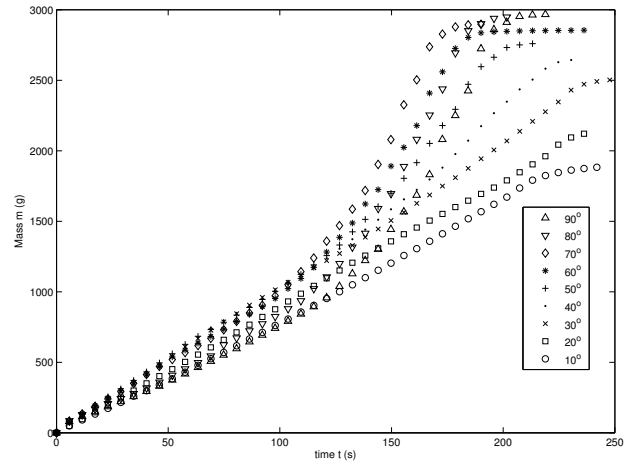
(a) Tank, Tube 2,  $\theta = 90^\circ$



(b) Tank, Tube 2,  $\theta = 40^\circ$



(c) Tank, Tube 2,  $\theta = 20^\circ$

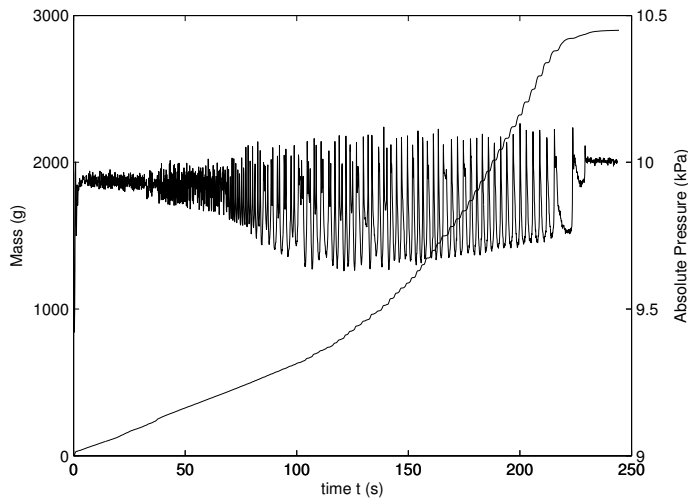


(d) Tank, Tube 2, mass flux for various angles

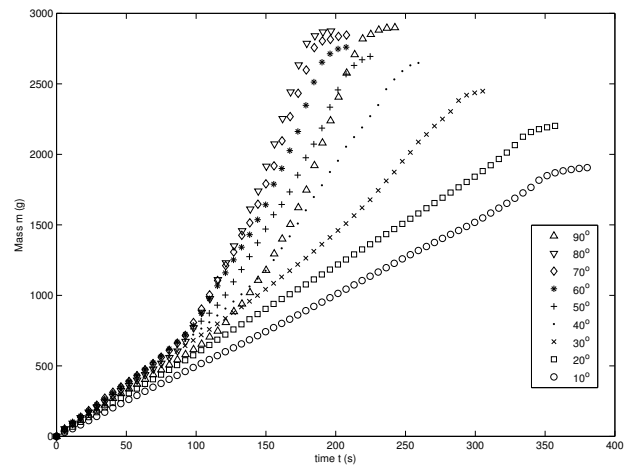
Figure 8: Tank with Tube 2

We now look at results for Tube 2. We first examine the effect of changing  $\theta$ . Figure 8a shows the  $\theta = 90^\circ$  data, and we clearly see the three regimes of ‘popping’, ‘glugging’ and ‘slugging’, along with step-like mass plot for the slugging phase. In Figure 8b we reduce  $\theta$  to  $40^\circ$ . We note there are still three distinct phases, although the amplitude of oscillation has decreased, and the step-like nature of the mass plot is less visible. Decreasing the angle further to  $\theta = 20^\circ$ , in Figure 8c, we see the three phases have been replaced with a (slightly noisy), linear shallow pressure, which steadily increases slowly with time, with small amplitude, high frequency oscillations. It thus appears, the three phases are not observed in the low angle regime.

Figure 8d shows the plots of mass with time, for various angles. We see a noticeable increase in gradient for the large angles when the slugging phase begins, and a constant gradient throughout for the low angle regimes - this is to be compared with Figure 3c and Figure 3d where we noticed similar behaviour.



(a) Tank, Tube 3,  $90^\circ$



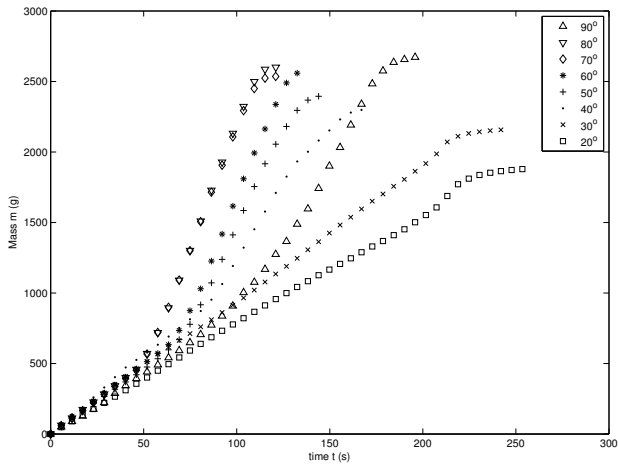
(b) Tank, Tube 3

Figure 9: Tank with Tube 3

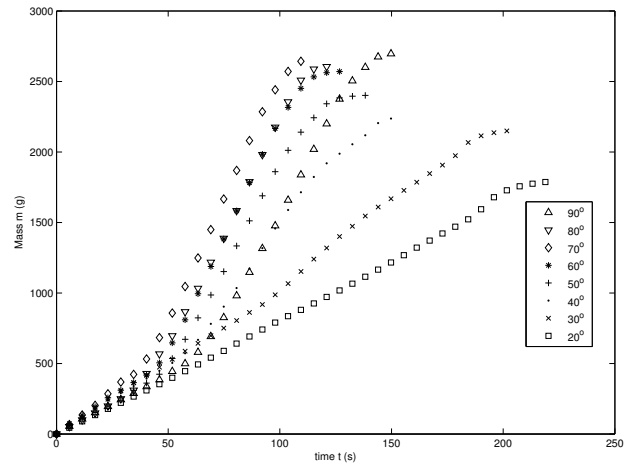
We now shorten the tube again to 50cm, using Tube 3. Figure 9a shows that three distinct phases still occur for  $\theta = 90^\circ$ , although the pressure oscillation amplitude in the slugging phase has decreased, and its frequency has increased, while the steps of the mass plot have become smaller and more frequent simultaneously. This is due to the shortening of the tube, which has the effect that the maximum length of drawdown is capped at a lower value, meaning less water is expelled and drawn back (and also less air following it) on each slug than for tube 2.

Figure 9b shows again a split in the data between the larger angles and the lower angles, for the mass-time plots, with larger angles experiencing larger gradients during the slugging phase, which the lower angles do not achieve.

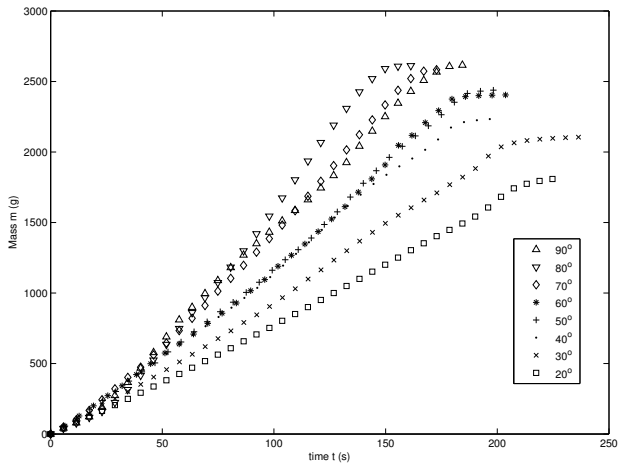
In Figure 10a, Figure 10b, and Figure 10c, I continually shorten the tube using Tubes 4, 5 and 6 respectively. I notice some trends between the graphs: in each, the data is split between low angle, non-slugging flow, and high angle slugging flow. This is less pronounced in Figure 10c, where the tube length is shortest, but there is a definite increase in gradient for large angles just before 50s. The time at which slugging begins decreases as tube length decreases, as the maximum length of drawdown reaches its cap at a shorter distance.



(a) Tank, Tube 4



(b) Tank, Tube 5



(c) Tank, Tube 6

Figure 10: Tank with Tube 4, 5 and 6

## Theory

In this section, I present a theoretical model for one glug of Experiment 2. This model ignores viscous effects. Figure 11 shows a diagram of the terms used henceforth.

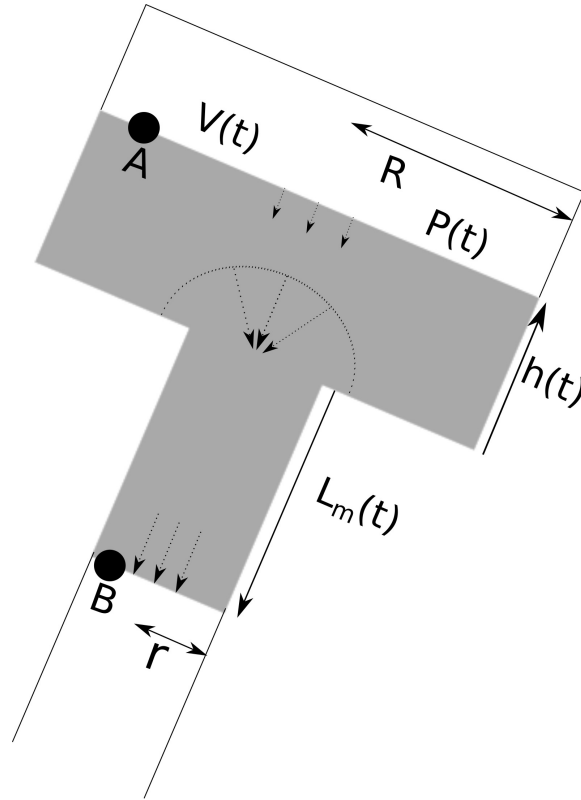


Figure 11: Theoretical Diagram

Define:

|   |                               |
|---|-------------------------------|
| $V(t)$ = volume of air in tank at time $t$ ,                          | $V(0) = V_0$                  |
| $h(t)$ = height of water in tank at time $t$ ,                        | $h(0) = h_0$                  |
| $P(t)$ = Pressure above water surface in tank,                        | $P(0) = P_0$ , atmospheric    |
| $L_m(t)$ = length of water in tube, accounting for finite tube length | $L(0) = 0$                    |
| $m(t)$ = mass of water in bucket at time $t$                          | $L_1 = \text{Length of tube}$ |
| $u(t)$ = velocity of lower free surface in tube                       |                               |
| $R$ = radius of tank  |                               |
| $r$ = radius of tube  |                               |
| $\gamma$ = heat capacity ratio  |                               |
| $A$ = point on top free surface                                       |                               |
| $B$ = point on lower free surface                                     |                               |

We begin by considering a vertical tank ( $\theta = 90^\circ$ ). Consider one cycle of glugging, beginning with outflow, where the position of the meniscus is at rest above the hole when  $t=0$ .

Conservation of volume:

$$\begin{aligned}
\frac{dV}{dt} &= -\pi R^2 \frac{dh}{dt} & \pi R^2 \frac{dh}{dt} &= -\pi r^2 \frac{dL_m}{dt} \\
\Rightarrow V - V_0 &= \pi R^2 (h_0 - h) & \Rightarrow R^2 (h - h_0) &= -r^2 L_m \\
\Rightarrow \frac{V}{V_0} &= 1 + \frac{\pi r^2 (h_0 - h)}{V_0} & \Rightarrow L_m &= \frac{R^2}{r^2} (h_0 - h)
\end{aligned}$$

Following Clanet, since the period of oscillation is (of the order of the second) compared to the time of thermal equilibrium,  $4R^2/D_{th}$  where  $D_{th}$  is the thermal diffusivity of air, we can assume the expansion of air is isentropic:

$$PV^\gamma = P_0 V_0^\gamma$$

$$\Rightarrow P = P_0 \left( 1 + \frac{\pi R^2}{V_0} [h_0 - h] \right)^{-\gamma} \quad (1)$$

By mass conservation, before the lower free surface reaches the end of the tube, the velocity at B is

$$u = -\frac{R^2}{r^2} \frac{dh}{dt} \quad (2)$$

We are to assume we have unsteady, potential flow, where we can apply Bernoulli's theorem to the points A and B on the upper and lower free surfaces respectively. To evaluate the potential, we assume the flow has the structure presented in Figure 11.

Taking  $x$  measured downwards, in (the majority of) the tank, we have uniform flow,  $U$  in the  $x$  direction, giving:

$$\begin{aligned}
U &= \frac{r^2}{R^2} u \\
\Rightarrow \phi_1 &= \frac{r^2}{R^2} ux
\end{aligned}$$

In the lower part of the tank, just above the tube we assume radial sink flow:

$$\phi_2 = \frac{q}{4\pi r}$$

where  $q$  is the flux due to a hemisphere just above the tube, so that  $q = 2\pi r^2 u$

$$\begin{aligned}
\Rightarrow \phi_2 &= \frac{\pi r u}{2} \\
\Rightarrow \frac{d\phi_2}{dt} &= \frac{\pi r}{2} \frac{du}{dt}
\end{aligned}$$

In the tube, we have uniform flow:

$$\phi_3 = ux$$

We can set  $\frac{d\phi_1}{dt} = 0$  on the upper surface by making a transformation involving a function of time only. Adding  $\phi = \phi_2 + \phi_3$  for the lower surface, and differentiating and evaluating at  $x = L_m$  gives:

$$\Rightarrow \frac{d\phi}{dt} = \frac{du}{dt} \left( \frac{\pi r}{2} + L_m \right)$$

We assume that  $r \ll R$  so that  $U^2 \ll u^2$  giving the Bernoulli equation:

$$P + \rho gh = -\rho \frac{du}{dt} \left( \frac{\pi r}{2} + L_m \right) + \frac{1}{2} \rho u^2 + P_0 - \rho g L_m$$

I now insert equations (1) and (2) for  $P$  and  $u$  respectively and rearrange to give the following 2<sup>nd</sup> order, non-linear equation for  $h$ , noting that  $L_m$  is related to  $h$  also:

$$\Rightarrow \rho \frac{R^2}{r^2} \left( \frac{\pi r}{2} + L_m \right) \ddot{h} = \rho \frac{R^4}{2r^4} \dot{h}^2 + P_0 \left[ 1 - \left( 1 + \frac{\pi R^2}{V_0} [h_0 - h] \right)^{-\gamma} \right] - \rho g (h + L_m)$$

Where the dots represent time derivatives with respect to  $t$ . Interpretation of this equation: the term on the left hand side is the acceleration of the fluid height. The first term on the left hand side represents the inertia of the fluid. The second term accounts for the strength of the vacuum above the water in the tank acting to pull the fluid backwards as it begins to accelerate down the tube. The last term is the hydrostatic pressure head.

I now non-dimensionalize the problem, scaling  $h$  as:

$$\begin{aligned} \frac{\pi R^2}{V_0} (h_0 - h) &= -y \\ \Rightarrow \rho \frac{V_0}{\pi r^2} \left( \frac{\pi r}{2} + L_m \right) \ddot{y} &= \rho \frac{V_0^2}{2\pi^2 r^4} \dot{y}^2 + P_0 \left[ 1 - (1 - y)^{-\gamma} \right] - \rho g \left( h_0 + \frac{V_0}{\pi R^2} y + L_m \right) \end{aligned}$$

From the first term on the RHS, I choose to scale  $t$  as:

$$t = \left( \frac{\rho V_0^2}{P_0 \pi^2 r^4} \right)^{1/2} \tau$$

and, by representing differentiation with respect to  $\tau$  by primes obtain:

$$\Rightarrow \frac{\pi r^2}{V_0} \left( \frac{\pi r}{2} + L_m \right) y'' = \frac{1}{2} (y')^2 + \left[ 1 - (1 - y)^{-\gamma} \right] - \frac{1}{H_0} \left( h_0 + \frac{V_0}{\pi R^2} y + L_m \right) \quad (3)$$

Where

$$H_0 = \frac{P_0}{\rho g}$$

is the height associated with the pressure head.

During outflow

$$L_m = \min \left[ L_1, -\frac{V_0 y}{\pi r^2} \right]$$

And during inflow

$$L_m = L_1 - \frac{V_0}{\pi r^2} (y - y_0)$$

Where  $y_0$  is the value of  $y$  when outflow stops, and inflow begins.

I solve this numerically (taking as typical initial conditions  $h_0 = 0.11m$ ,  $V_0 = 0.0023m^3$ ), and present the results in Figure 12. I see that once  $L_m$  reaches  $L_1$ ,  $m$  begins to increase, while  $h$  and  $P$  decrease. At the minimum height  $h = 0.099$ ,  $L_m$  draws back from  $L_1$ , while  $m$  flattens out, and  $P$  increases again. When  $L_m = 0$  again,  $h$  and  $P$  have returned to less than  $h_0$  and  $P_0$  respectively, and the program stops, as another model is needed to simulate the entry of air into the tank.

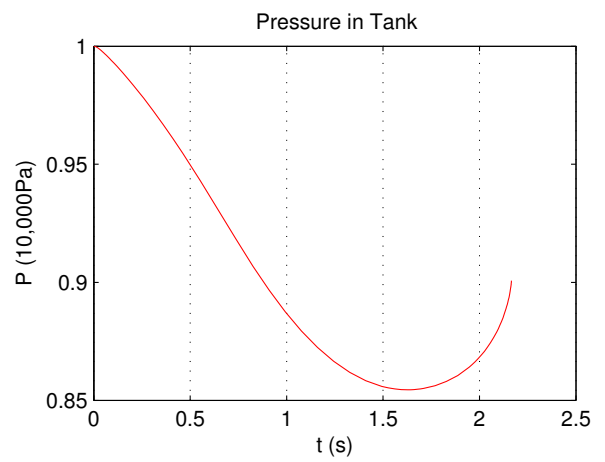
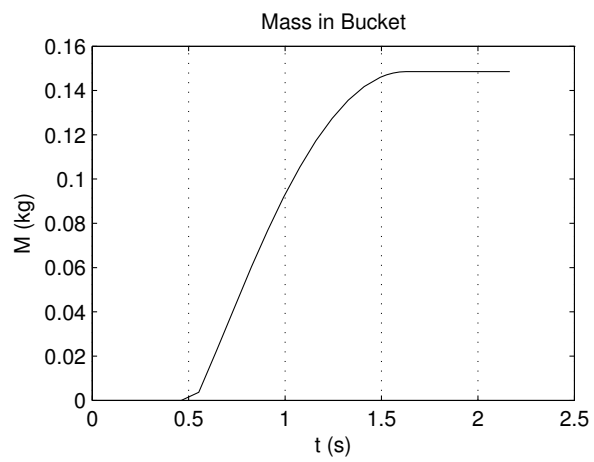
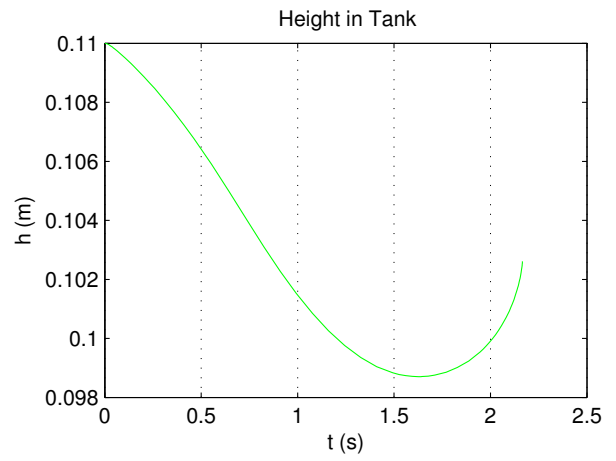
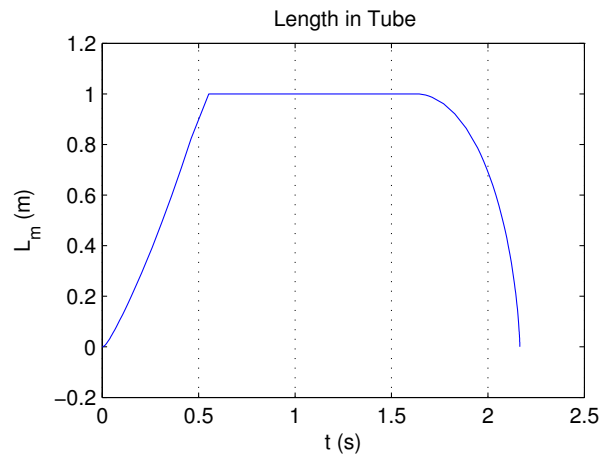


Figure 12: Numerical Results